Multimodal visualization of adult stem cells in inner ear and brain pathology

Schomann, T.

Citation

Schomann, T. (2019, May 16). *Multimodal visualization of adult stem cells in inner ear and brain pathology.* Retrieved from https://hdl.handle.net/1887/72413

Version:	Not Applicable (or Unknown)
License:	[Leiden University Non-exclusive license](https://hdl.handle.net/1887/72413)
Downloaded from:	https://hdl.handle.net/1887/72413

Note: To cite this publication please use the final published version (if applicable).

Cover Page

The following handle holds various files of this Leiden University dissertation:
http://hdl.handle.net/1887/72413

Author: Schomann, T.
Title: Multimodal visualization of adult stem cells in inner ear and brain pathology
Issue Date: 2019-05-16

Chapter 3

Lentiviral transduction and subsequent loading with nanoparticles do not affect cell viability and proliferation in hair-follicle-bulge-derived stem cells *in vitro*

T. Schomann, L. Mezzanotte, I.M. Lourens, J.C.M.J. de Groot, J.H.M. Frijns, M.A. Huisman

Abstract

The application of stem cells in the treatment of various degenerative diseases is highly promising. However, cell-based therapy could be limited by the problem of low viability of grafted cells and uncertainty about their fate. The combination of molecular imaging and contrast-enhanced MRI may give more insight into the survival and behavior of grafted stem cells. We explore hair-follicle-bulge-derived stem cells (HFBSCs) as a potential candidate for autologous cell-based therapy. HFBSCs are transduced with a lentiviral construct with genes coding for bioluminescent (Luc2) and fluorescent (copGFP) reporter proteins, and subsequently loaded with magnetic nanoparticles to enable MRI visualization. Thus, we investigate for the first time if lentiviral transduction and cellular loading with nanoparticles have a cytotoxic effect upon these stem cells. Transduction efficiency, proliferation rate, cell viability and reporter protein co-expression during long-term culture of transduced HFBSCs were studied using fluorescence and bioluminescence microscopy. In addition, the effect of TMSR50 nanoparticles on proliferation and viability was investigated using the MTS assay and bioluminescence microscopy. The amount of TMSR50-loaded HFBSCs needed to reach signal threshold for MRI was assessed using an agarose phantom. Transduction with the Luc2-copGFP construct did not influence senescence, proliferation, doubling time, and differentiation of the HFBSCs. CopGFP expression was visible immediately after transduction and persisted for at least 15 passages, concomitantly with Luc2 expression. Cellular loading with TMSR50 nanoparticles did not affect cell viability and proliferation. The results imply that combined MRI and bioluminescence imaging may enable *in vivo* localization and long-term monitoring of grafted viable HFBSCs.

Introduction

1

In regenerative medicine, stem cells are a promising therapeutic tool to treat disorders for which no effective treatments are currently available, such as neurocardiovascular, neurodegenerative, hematologic, immunodeficiency diseases and many more [1-6]. Since low post-transplantation survival rates remain a major problem [7], the assessment of the actual effectiveness of cell-based therapy may be limited by the inability to detect and monitor stem cells after engraftment in the living host. Hence, research has focused on *in vivo* visualization of genetically manipulated (transduced) cells and/or cells containing contrast agents (e.g. magnetic nanoparticles) using a variety of imaging modalities including bioluminescence and fluorescence imaging as well as contrast-enhanced magnetic resonance imaging (MRI). Longitudinal preclinical investigation regarding the cytotoxic effects of genetic manipulation and/ or nanoparticle-loading of the stem cells is therefore a prerequisite.

2

3

Bioluminescence imaging makes use of firefly or click beetle luciferases which enzymatically convert the substrate D-luciferin into oxyluciferin, resulting in a bioluminescent signal emitting at a wavelength of 425–550 nm [8-10]. Importantly, bioluminescence imaging allows the monitoring of living cells due to the requirement of O_2 and ATP. Since light in this range (blue to green) is particularly well-absorbed by tissue chromophores, such as (oxy-)hemoglobin, melanin and cytochromes, these wildtype luciferases have limited value for in vivo imaging applications [11, 12]. The codon-optimized firefly luciferase Luc2, however, is a good alternative. It couples a high photon flux at its emission peak of 560 nm (at 25 °C) with a thermally induced shift in wavelength (610 nm at 37 °C) – which is beyond the light absorption spectrum of mammalian tissue – and, hence, rendering it a valuable tool for in vivo bioluminescence imaging [13].

4

5

6

An alternative approach is to monitor cells by means of fluorescence imaging using naturally occurring fluorescent proteins, such as green fluorescent protein (GFP) and its numerous variants [14-17]. One of these is copepod green fluorescent protein (copGFP), which occurs in marine planktonic crustaceans belonging to the copepod families Pontellidae and Aetideidae [18, 19]. One of the advantages of copGFP (λ_{ex}: 482 nm, λ_{em}: 502 nm) is that it can be detected in copGFP-expressing cells during cell culture and in histological sections using conventional fluorescence microscopy. In addition, it demonstrates a high fluorescence quantum yield, is more stable at a

7

8

A

wide range of temperatures (including 37 °C, i.e. mammalian body temperature), and features faster folding and faster post-translational maturation rates resulting in rapid availability of the protein after transduction [20].

Bioluminescence and fluorescence imaging, however, do not provide detailed anatomical information. In contrast, MRI of transduced cells loaded with contrast-enhancing nanoparticles allows in vivo monitoring of their exact location and migration within the host after engraftment [21-24]. Recently, multimodal imaging probes that facilitate visualization by means of fluorescence imaging and microscopy as well as MRI have been developed.

NEO-STEM™ TMSR50 nanoparticles are such dual probes, consisting of a magnetic cobalt-ferrite core surrounded by a degradation-resistant silica shell containing the red-fluorescent (625 nm) dye rhodamine B isothiocyanate [25, 26]. TMSR50 nanoparticles are biocompatible with adenocarcinomic A549 cells and human umbilical-cord-blood-derived mesenchymal stem cells [25, 27, 28], but their biocompatibility has not been verified for stem cells from other sources, such as hair-follicle-bulge-derived stem cells (HFBSCs). These stem cells originate from the neural crest [29] and are a promising source of non-embryonic stem cells to be used in autologous cell-based therapy, by virtue of their broad regenerative potential and non-oncogenic properties as well as the fact that they are relatively easy to harvest [30-33].

The present study was designed to test in detail if lentiviral transduction followed by nanoparticle loading have a cytotoxic effect upon HFBSCs intended for grafting. The aim of this study was to get an understanding of the usability of bioluminescence and fluorescence imaging and MRI, in order to visualize and longitudinally monitor viable HFBSCs within live animals after engraftment. Therefore, HFBSCs were transduced with a lentiviral dual-reporter gene construct containing genes that code for Luc2 and copGFP, which are expressed at an equimolar ratio [34], and subsequently loaded with TMSR50 nanoparticles. This allows verification of transduction efficiency and monitoring of the persistence of reporter molecules during culture. Since a possible cytotoxic effect of lentiviral transduction and cellular loading with nanoparticles cannot be excluded [35-37], we have investigated whether or not these treatments affect the proliferation rate, doubling time, cellular senescence, apoptotic pathways and long-term viability of HFBSCs.

Results

Transduced HFBSCs demonstrate stable co-expression of reporter molecules

Expression of the bioluminescent (Luc2) and the fluorescent reporter molecule (copGFP) was monitored over several passages. Expression of copGFP was observed at all selected time points, starting immediately after transduction (P1) and persisting up to P15 (Fig. 1). The majority of targeted cells expressed a green-fluorescent signal (mean ± SEM: 83.6 ± 8.2%).

Transduced HFBSCs stably co-express both reporter molecules as bioluminescence microscopy demonstrated that after addition of D-luciferin a bioluminescent signal indicative of Luc2 activity could be recorded at high passages after transduction (P10 and P15; Fig. 1).
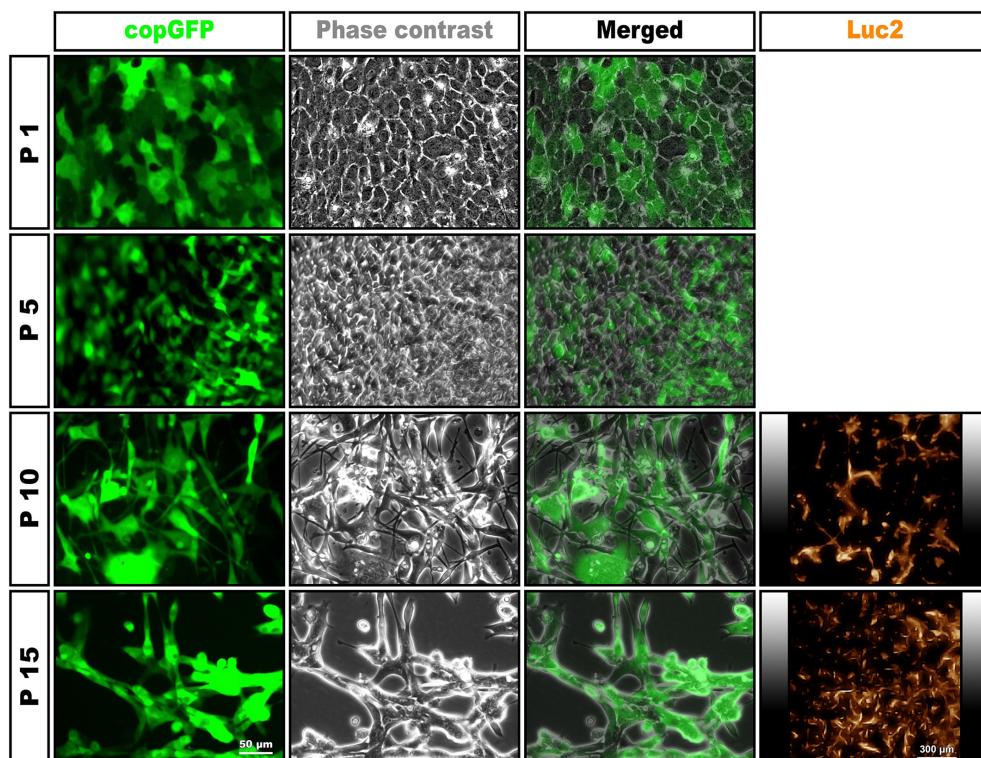
Fig. 1: Stable co-expression of copGFP and Luc2. After lentiviral transduction with the Luc2-copGFP reporter gene construct, the majority of cells exhibit green fluorescence indicating copGFP expression. The fluorescent signal persists for at least 15 passages (P15). Addition of D-luciferin results in a bioluminescent signal due to luciferase activity at P10 and P15, confirming co-expression of Luc2. Scale bar = 50 μm (copGFP, phase contrast, and merged images) or 300 μm (Luc2 images).

Transduction does not inhibit HFBSC proliferation

The proliferation rates of transduced HFBSCs and non-transduced control cells were compared at 1 day, 2 and 3 days (Fig. 2A). Data analysis shows that proliferation curves for the transduced and control cells do not differ in a statistically significant way (p = 0.921, two-tailed, unpaired *t*-test, 95% confidence interval, n = 12 per data point).

The doubling time averages 36.5 ± 3.9 hours for transduced cells and 37.3 ± 6.7 hours for control cells (Fig. 2B), but this difference is statistically not significant (p = 0.894, two-tailed, unpaired *t*-test, 95% confidence interval, n = 9).
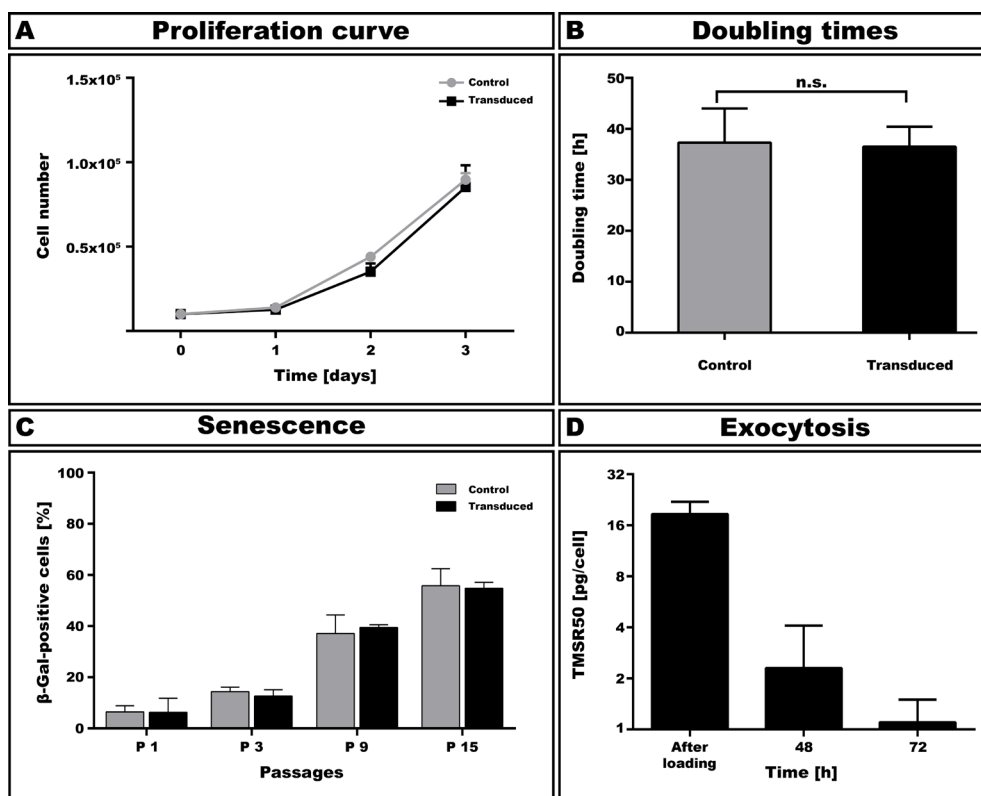
Fig. 2: Transduction does not interfere with HFBSC proliferation and senescence. **A:** The proliferation rate of transduced HFBSCs does not significantly differ from that of non-transduced (control) cells after 1 day, 2 and 3 days (error bars: standard error of the means, SEM). **B:** Comparison of the doubling times of transduced and control cells does not reveal statistically significant differences (error bars: SEM). **C:** Enzyme histochemical staining for lysosomal β-galactosidase reveals that transduced and control cells become senescent alike. The percentage of blue-stained cells increases stably over 15 passages for both the control and transduced cells (error bars: SEM). **D:** Exocytosis and retention of nanoparticles per cell over time reveals robust decrease in TMSR50 concentration per cell within 48 hours. As shown, the concentration of nanoparticles within each cells decreased slightly at 72 hours. At 96 hours after loading, exocytosis of TMSR50 nanoparticles by the cells into the medium was below detectable threshold.

Exocytosis and retention of TMSR50 nanoparticles in transduced HFBSCs

Exocytosis of nanoparticles was followed after loading of transduced HFBSCs. Red fluorescence of TMSR50 nanoparticles in medium was measured directly after loading, 48 hours and 72 hours after loading. Directly after loading, supernatant contained 0.1905 ± 0.0112 mg/ml TMSR50 (Fig. 2D). The nanoparticle concentration in medium was 0.0041± 0.0016 mg/ml after 48 hours and 0.0004 ± 0.0007 mg/ml after 72 hours. At later time points, no fluorescence could be measured.

Knowing the amount of initially seeded cells and the doubling time of 36.5 hours, we were able to calculate the average concentration of uptaken nanoparticles. Directly after loading cells contained 18.6 ± 3.4 pg/cell, while after 48 hours and 72 hours they contained 2.3 ± 1.8 pg/cell and 1.1 ± 0.5 pg/cell, respectively. At 96 hours after loading, fluorescence of exocytosed TMSR50 nanoparticles in the medium was below detectable threshold.

Intracellular retention of nanoparticles was followed in transduced HFBSCs at two different densities (1.0×10^4 and 7.5×10^4 cells/well) over a subsequent period of 7 days. After 1 day, all cells showed red fluorescence indicative of intracellular accumulations of TMSR50 nanoparticles (Fig. 3A–B). Merged images indicate that copGFP and TMSR50 nanoparticles co-exist in the cells. Phase contrast images reveal that the cells remain a normal morphology throughout the 7-day period of observation. Three days after loading, a considerable loss of the red-fluorescent signal was observed in cultures seeded at a density of 1.0×10^4 cells/well (Fig. 3C), whereas cells seeded at 7.5×10^4 cells/well did retain a strong red-fluorescent signal (Fig. 3D). After seven days, the red-fluorescent signal had declined for both densities (Fig. 3E–F), although the cells seeded at 7.5×10^4 cells/well demonstrated a higher signal.

TMSR50 nanoparticles do not induce apoptosis-related caspase activity

We investigated the possible cytotoxic effect of the TMSR50 nanoparticles upon transduced HFBSCs by monitoring caspase-3/7 and caspase-9 activities during the initial 24 hours of cell loading with TMSR50 nanoparticles (Fig. 4A). Caspase-3/7 and caspase-9 activities in TMSR50-loaded cells were not different in a statistically

1

2

3

4

5

6

7

8

A

significant way from those in non-loaded transduced cells (caspase-3/7: p = 0.072, caspase-9: p = 0.699; two-tailed, paired t-tests, 95% confidence interval, n = 6). These results demonstrate that TMSR50 nanoparticles do not activate caspase-3/7-mediated or caspase-9-mediated apoptosis in HFBSCs.
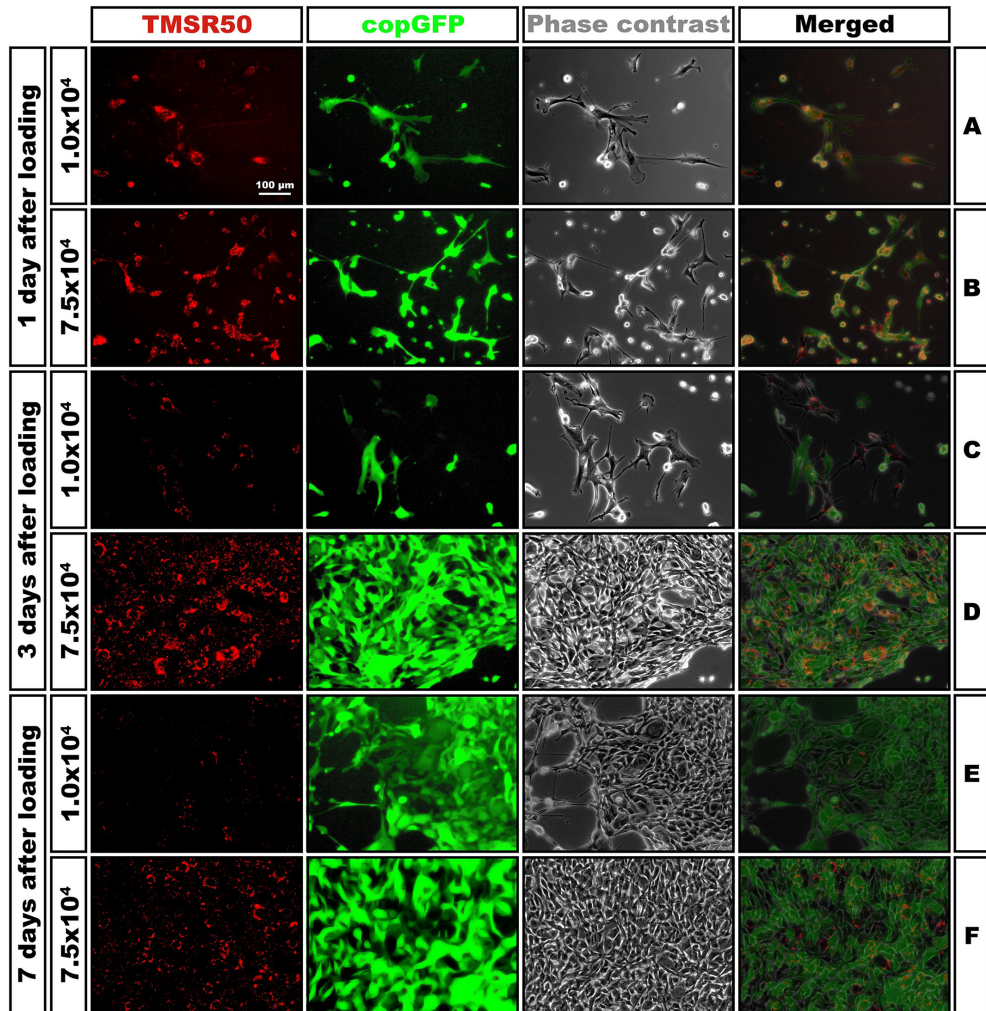
Fig. 3: Intracellular retention of TMSR50 nanoparticles in transduced HFBSCs. Intracellular retention of red-fluorescent TMSR50 nanoparticles was monitored in transduced HFBSCs at seeding densities of 1 × 10^4 (**A**, **C**, **E**) and 7.5 × 10^4 cells/well (**B**, **D**, **F**) for up to seven days. From the merged images it is evident that copGFP and TMSR50 co-exist in the cells. Loss of red fluorescence was observed in cultures at 1 × 10^4 cells/well after three and seven days (**C**, **E**). Red-fluorescent signal was retained in cultures seeded at 7.5 × 10^4 cells/well for up to seven days (**D**, **F**). Scale bar = 100 μm.
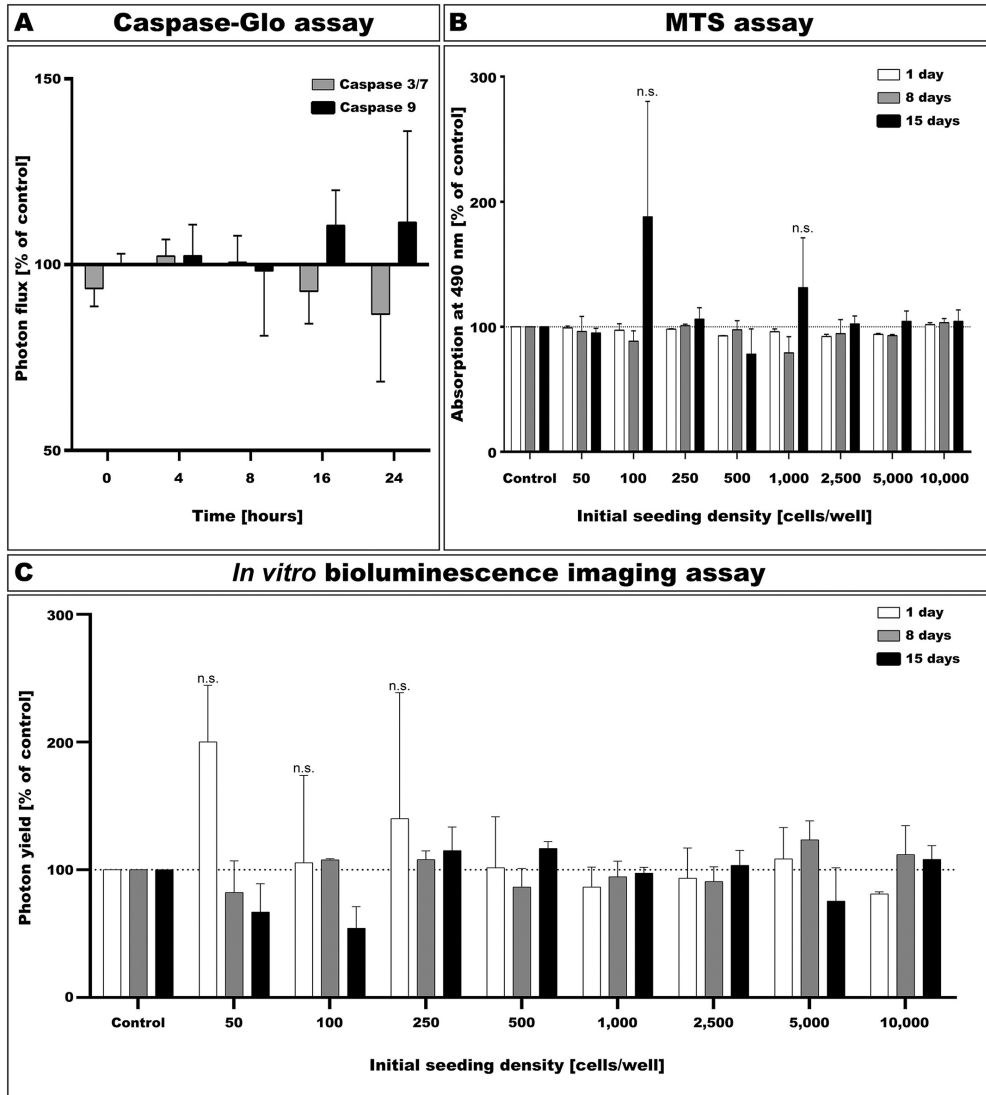
Fig. 4: TMSR50 nanoparticles do not reduce HFBSC viability. **A:** Loading with TMSR50 nanoparticles does not result in significant increases in caspase-3/7 or caspase-9 activities in HFBSCs over a period of up to 24 hours. Bioluminescence of the cells is expressed as a percentage of the photon flux normalized to that of non-loaded transduced cells (100% line; error bars: SEM). **B:** MTS assay demonstrates that viability of transduced HFBSCs is not significantly reduced by TMSR50 nanoparticles after one day or after eight and 15 days. Data are expressed as percentage of absorption at 490 nm and normalized to that of non-loaded transduced cells (control: dotted line; error bars: SEM). **C:** Results with *in vitro* bioluminescence imaging are similar to those obtained with the MTS assay. Data are expressed as percentage of photon yield normalized to the non-loaded transduced cells (control: dotted line; error bars: SEM).

57

Intracellular TMSR50 nanoparticles do not reduce HFBSC viability

Viability of transduced HFBSCs loaded with TMSR50 nanoparticles was investigated at different densities (range: 0.5×10^2 thru 1.0×10^4 cells/well) over a period of 15 days using the MTS assay and *in vitro* bioluminescence imaging.

Statistical analysis of the data obtained with the MTS assay (Fig. 4B) could not demonstrate any statistically significant changes between the different cell densities as compared to non-loaded transduced HFBSCs, not even after prolonged incubation for up to 15 days (p = 0.379, 3-way ANOVA, one-sample *t*-test, 95% confidence interval, n = 6 per data point).

Fig. 4C graphs the normalized data after bioluminescence imaging for the different densities of transduced HFBSCs loaded with TMSR50 nanoparticles. Similar to the MTS data, no statistically significant differences could be observed (p = 0.531, 3-way ANOVA, one-sample *t*-test, 95% confidence interval; error bars: SEM, n = 6 per data point).

TMSR50-loaded and non-loaded HFBSCs differentiate alike

Following the differentiation protocol established by Gho *et al*. [38], different neuron-like cells with elongated, branched projections developed over time (Fig. 5). In comparison, no differences were observed regarding the differentiation potential between TMSR50-loaded and non-loaded HFBSCs regarding their morphology. While all cells contain nanoparticles after differentiation (e.g. Fig. 5, arrowhead), not all cells are transduced. However, differentiated transduced cells were also loaded with TMSR50 nanoparticles as indicated by red fluorescence (Fig. 5, circle).

MRI of agarose-embedded TMSR50-loaded HFBSCs

Transduced HFBSCs loaded with TMSR50 nanoparticles were embedded in a multi-layered agarose phantom containing a cell gradient (1.0×10^6, 1.0×10^5, $1.0 \times 10^{4,}$ and 1.0×10^3 cells/layer) and investigated using *in vitro* fluorescence imaging and MRI.

Lentiviral transduction and subsequent loading with nanoparticles do not affect cell viability and proliferation in hair-follicle-bulge-derived stem cells *in vitro*
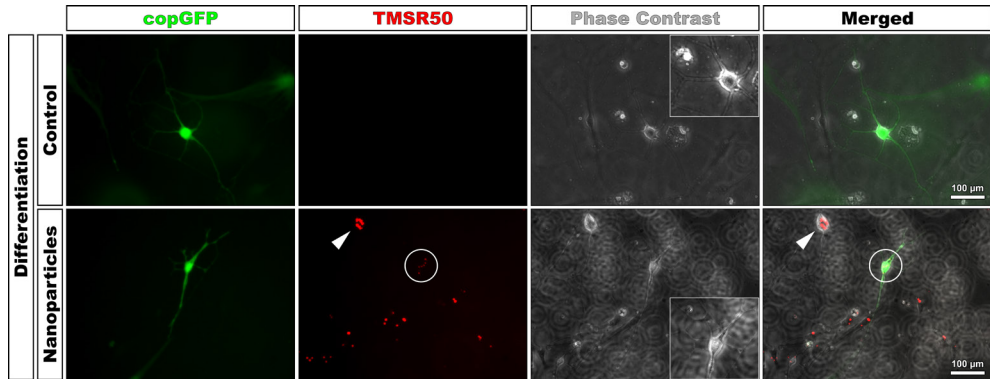
Fig. 5: TMSR50-loaded and non-loaded HFBSCs differentiate alike. Non-loaded (control) and TMSR50-loaded (nanoparticles) HFBSCs were differentiated. After differentiation, both groups developed the same morphologies. The neuronal differentiation process occurred similarly in cells with and without nanoparticles. In both cultures the cells formed networks (see magnified phase contrast). While no red fluorescence was observed in control cells, TMSR50-loaded cells contain red-fluorescent nanoparticles. Scale bar = 100 µm.
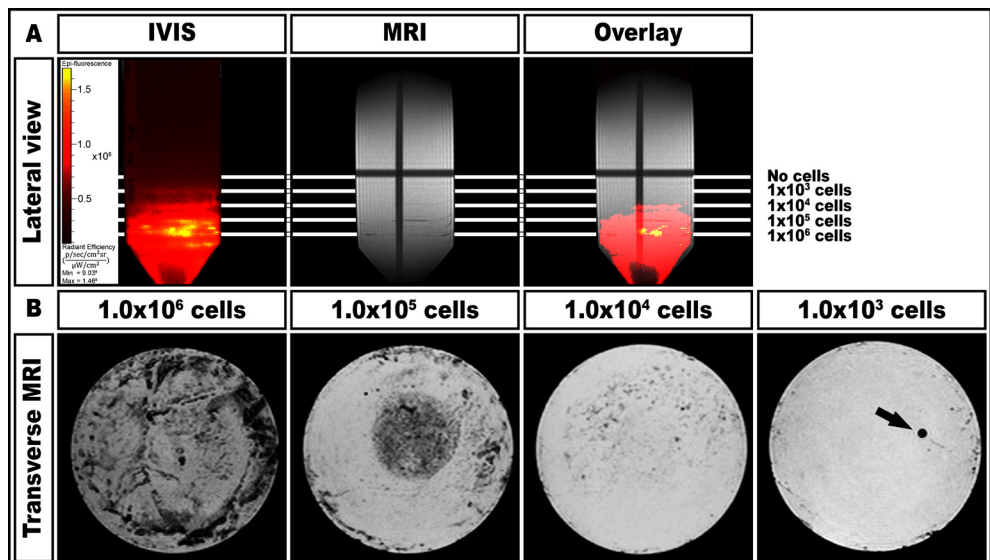
Fig. 6: Visualization of different amounts of TMSR50-loaded HFBSCs. **A:** Images (lateral view) of the 0.5% agarose phantom show layers containing different amounts of TMSR50-loaded HFBSCs (1×10^3 to 1×10^6 cells/layer). Left image: cells visualized by epi-fluorescence imaging with the IVIS® Spectrum multimodal imaging system (min = 9.036, max = 1.468); middle image: cells visualized by contrast-enhanced MRI; and right image: overlay of both. With fluorescence imaging a signal emerges from all cell-containing layers. The layer without TMRS50-loaded HFBSCs does not exhibit fluorescence. MRI displays three distinct layers (1×10^6, 1×10^5 and 1×10^4 cells/layer). The layer containing 1×10^3 cells does not yield sufficient contrast, nor does the layer without cells. **B:** Transverse MRI view of the phantom layers containing TMSR50-loaded HFBSCs. For each image, three consecutive transverse MRI slices of the respective layers were merged. The layers containing 1×10^5 cells and, especially, 1×10^6 cells were clearly above the detection limit, whereas 1×10^4 cells only gave faint contrast. While 1×10^3 cells/layer could be visualized by fluorescence imaging, this amount revealed few hypointense spots (apart from an air bubble right from the center: arrow) at the periphery of the agarose phantom using MRI.

Fluorescence imaging revealed a strong, red-fluorescent signal in the layers containing 1.0×10^6 and 1.0×10^5 cells, whereas the intensity of the signal was distinctly visible in the layers with 1.0×10^4 and 1.0×10^3 cells (Fig. 6A, IVIS).

The agarose phantom was also subjected to MRI and in the lateral view the layers containing 1.0×10^6, 1.0×10^5 and 1.0×10^4 cells show sufficient contrast to allow visualization of the different cell layers (Fig. 6A, MRI). In the transverse view of the MRI (Fig. 6B), the layers containing the higher amounts of cells (1.0×10^6 and 1.0×10^5, respectively) showed clear hypointense spots, whereas the layer with 1.0×10^4 cells was only faintly visible. The layer containing 1.0×10^3 cells shows few hypointense spots at the periphery of the phantom.

Autofluorescence or false-positive MRI signal can be ruled out for the imaged layers, since the layer without cells did not give any signal, either with IVIS or with MRI (Fig. 6A).

Discussion

In this study, we demonstrated that the stem cell population derived from the hair follicle bulge of mouse whisker pads can be stably transduced with the Luc2-copGFP reporter gene construct using a lentiviral vector, allowing fluorescence and bioluminescence imaging. In addition, cells retained the ability to express these reporter molecules after cryopreservation. Furthermore, cells can be efficiently loaded with TMSR50 nanoparticles enabling visualization in an agarose phantom using contrast-enhanced MRI indicating suitability for longitudinal preclinical studies *in vivo*.

The stable integration of the lentiviral construct within the genome of the HFBSCs was evidenced by equimolar co-expression of Luc2 and copGFP for at least 15 passages after transduction. Unlike previous studies [35-37], we did not observe any effect of the transduction upon cell morphology, proliferation, including doubling times, and degree of senescence during these long-term cultures. This discrepancy could be explained by the use of different (stem) cell types. In our study, we have used HFBSCs, whereas in the other papers other cell types and cell lines have been used, such as fibroblasts [32], neuroblastoma cells [35] and mesenchymal stem cells [36]. Alternative explanations could be the use of different GFP variants (GFP versus copGFP) and different viral transduction methods.

After excluding possible inhibitory effects of viral transduction with Luc2-copGFP, we investigated if additional loading with silica-coated nanoparticles triggers the apoptosis-related caspase-3/7 or caspase-9 pathways, as reported previously by Kai *et al*. [39]. Our results have shown that neither caspase-3/7 nor caspase-9 activities are significantly increased when compared to control cells within 24 hours, not even in the first 8 hours after the start of the loading procedure.

Also, we investigated uptake and exocytosis of TMSR50 nanoparticles by HFBSCs. We found that the initial concentration of nanoparticles is in average 18.6 pg/cell and steeply decreases in the following 48 hours. However, the amount of exocytosed nanoparticles stabilized thereafter. After this the amount of exocytosed nanoparticles is not measurable anymore, making cell proliferation the main factor for decrease of nanoparticle concentration in the cells.

1

2

3

4

5

6

7

8

A

In addition, we checked if TMSR50 nanoparticles persist in transduced HFBSCs during 7-day culturing, by monitoring the cell cultures with *in vitro* fluorescence microscopy. After 3 days, cultures containing 1.0×10^4 cells demonstrated slightly less red fluorescence than the cultures containing 7.5×10^4 cells. The 7-day cultures with 7.5×10^4 cells demonstrated a distinct red-fluorescent signal, while the corresponding culture with 1.0×10^4 cells revealed only a faint signal. It is generally known from pulse-chase studies that the amount of intracellular nanoparticles decreases due to dilution during proliferation. In addition, the total amount of nanoparticles in the culture containing 1.0×10^4 cells further decreases due to exocytosis and subsequent medium changes and this explains the pronounced reduction of fluorescent signal in these cultures as compared to the ones containing 7.5×10^4 cells. Therefore, future *in vitro* and *in vivo* nanoparticle-loading experiments should be done at relatively high seeding densities. Our results further indicate that MRI of TMSR50-loaded stem cells needs to be performed within seven days after transplantation, although Kallur *et al*. showed longer *in vivo* retention using different cells and nanoparticles [24]. It should be noted that there are more sensitive methods to detect iron oxide-loaded cells than the method described in this report. It has recently been shown that it is even possible to detect a small number of cells or even single cells, such as Kircher *et al*. following injection of nanoparticle-loaded sensitized T cells to tumor antigens [40]. Furthermore, Foster-Gareau *et al*. showed that single cells loaded with iron oxide nanoparticles could be imaged with a 1.5 T clinical scanner [41]. The sensitivity of detection in vivo depends on many factors, such as hardware, resolution of acquired images, the type of cell and its uptake of iron-oxide nanoparticles. However, we have chosen to perform a feasibility study to combine of Luc2-copGFP-transduced cells with fluorescent, magnetic nanoparticles because the technique is easy, does not require transfection reagents and the detection limit is sufficient for our future *in vivo* experiments. We, like many others, will transplant $>1 \times 10^6$ cells and if only 1% of these cells survive we will still be able to visualize them by means of MRI as demonstrated by Yeum *et al*. [42]. Taking these factors into account, our next goal was to investigate if these nanoparticles negatively affect HFBSC viability in long-term cultures. Statistically, there were no significant differences in viability between nanoparticle-loaded transduced cells and the respective control cells. Three-way ANOVA did not reveal any statistically significant differences between the various virus batches used (data not shown), the different initial seeding densities, and the different individual mice (data not shown), nor did we find differences due to duration of the culture period. Therefore, we pooled all data and performed a one-sample

t-test, which confirmed that the observed outliers in MTS assay and BLI assay are not statistically significant. In contrast to previous studies on the cytotoxic effects of nanoparticles [43, 44], the silica-coated TMSR50 nanoparticles used in this study do not affect HFBSC viability in the short run as well as on the long term. Our finding that amounts as low as 1×10^4 nanoparticle-loaded HFBSCs can be visualized in an agarose phantom indicates that engrafted HFBSCs may be visualized and monitored *in vivo* by means of contrast-enhanced MRI.

In order to longitudinally monitor viable HFBSCs *in vivo*, bioluminescence imaging and MRI represent viable tools for non-invasive visualization after engraftment. These techniques enable exact localization of grafted cells in the living animal in combination with long-term monitoring of their survival and fate. Our group intends to apply BLI and MRI to non-invasively monitor grafted stem cells and longitudinally follow their survival and fate in the cochleas of deafened animals.

Conclusion

We conclude that HFBSCs can be efficiently and stably transduced with the Luc2-copGFP construct, followed by subsequent nanoparticle loading, without affecting cell viability, proliferation and differentiation. This implies that a combined approach using bioluminescence imaging and MRI may enable *in vivo* localization of grafted cells. This multimodal visualization system makes it feasible to monitor transplanted stem cells and simultaneously obtain anatomical information.

1

2

3

4

5

6

7

8

A

Experimental

Animals

Healthy wildtype mice (C57Bl/6) were bred and housed in the Central Animal Facility of Leiden University Medical Center (LUMC). Male and female surplus animals (n = 7) of varying age served as a source for whisker pads, from which HFBSCs were isolated. The use of the animals was approved by the LUMC Animal Experiments Committee (DEC permit 10172).

Animal care and handling was in accordance with the guidelines and regulations as stipulated by the Dutch Experiments on Animals Act (WoD) and the European Directive on the Protection of Animals Used for Scientific Purposes (2010/63/EU).

Culture of hair follicle bulge explants

Hair follicles were dissected out from the whisker pads and the bulge region was excised as previously described [45, 38].

Cell-culture-treated 12-well plates (TPP Techno Plastic Products AG, Trasadingen, Austria) were coated with poly-D-lysine (PDL; Sigma-Aldrich, St. Louis, MO, USA; 0.01 mg/ml in distilled water) at 37°C for 30 minutes. After drying, plates were rehydrated with basic growth medium (BGM) at 37°C for 30 minutes. BGM consists of DMEM/Ham's F-12 1:1 (Biochrom AG, Berlin, Germany), 1% GlutaMax™ (100x; Gibco, Bleiswijk, The Netherlands) and 1% antibiotic/antimycotic solution (100x; Sigma-Aldrich) supplemented with 10% fetal bovine serum (FBS; Gibco), 2% B-27® supplement without vitamin A (50x; Gibco), 1% N-2 MAX media supplement (100x; R&D Systems™, Minneapolis, MN, USA), recombinant human basic fibroblast growth factor (20 ng/mL; R&D Systems), and recombinant human epidermal growth factor (20 ng/mL; R&D Systems).

After rehydration, medium was discarded and in each well one hair follicle bulge explant was placed. To prevent drying, a 20-µL drop of BGM was gently placed on top of the explants, which were then allowed to adhere to the bottom of the well in a humidified incubator at 37°C and 5% CO_2. After 60 minutes, another 20-µL drop

of BGM was carefully added to the moist explants, followed by adding 500 µL of the same medium to each well after another 60 minutes. Plates were incubated in a humidified incubator at 37°C and 5% CO_2 and, after four days, the cultures were examined on a daily basis to detect any outgrowth of cells from the explants. At the first sign of cell outgrowth, the medium was replaced with fresh medium followed by removal of the explants after three days.

Passaging and cryopreservation of HFBSCs

HFBSCs were continuously cultured until 70-80% confluence for each passage [38]. After each passage and proliferation cycle, the cells were washed with phosphate-buffered saline (PBS) and treated with a pre-warmed (37°C) balanced salt solution containing 0.05% trypsin and 0.02% EDTA.4Na (Gibco), for exactly two minutes. After centrifugation, the cells were counted and seeded at a proliferation density of approximately 2.5×10^3 cells/cm^2 in PDL-coated cell-culture-treated plates. Passaged cells were processed either directly for transduction or frozen and stored.

Prior to cryopreservation, cells were centrifuged and the pellet was resuspended in FBS (Gibco) containing 10% dimethyl sulfoxide (Sigma-Aldrich) at a concentration of 1×10^6 cells/mL and immediately frozen. The vitrified samples were stored either at -80°C for short periods of time or in liquid nitrogen for long-term storage. Prior to use, the vitrified samples were thawed in a water bath (37°C) followed by dilution in an excess volume of BGM.

Lentiviral transduction with the Luc2-copGFP reporter gene construct

HFBSCs were genetically engineered by genomic integration of the Luc2-copGFP reporter gene construct using lentiviral transduction. Vector production and transduction procedures have been described in detail previously [34]. We have used the third-generation lentiviral vector pCDH-EF1-MCS-T2A-copGFP (SBI System Biosciences, Mountain View, CA, USA) containing the elongation factor 1α (EF1α) promoter and the T2A sequences, resulting in equimolar expression of the Luc2 and copGFP genes. Lentiviral particles were produced by transfection of HEK-293 T packaging cells with three packaging plasmids (pCMV-VSVG, pMDLg-RRE, pRSV-

REV; Addgene, Cambridge, MA, USA) and the lentiviral vector plasmid. Supernatant containing lentiviral particles were collected after 48 and 72 hours. Subsequent quantification of virus was performed using a standard antigen-capture HIV p24 ELISA (ZeptoMetrix Corporation, NY, USA). Vector production and cell transduction were performed under appropriate biosafety level conditions (ML-II) in accordance with the National Biosafety Guidelines and Regulations for Research on Genetically Modified Organisms. Procedures and protocols were reviewed and approved by the LUMC Biosafety Committee (GMO permit 08-129).

HFBSCs were seeded in PDL-coated 12-well plates at a cell density of 2.5×10^4 cells/well and maintained in a humidified incubator at 37°C and 5% CO_2. After attachment was accomplished, the cells were transduced using a MOI (multiplicity of infection) of 10. HFBSC transduction was performed under appropriate biosafety level conditions (ML-II) in accordance with the National Biosafety Guidelines and Regulations for Research on Genetically Modified Organisms. Procedures and protocols were reviewed and approved by the LUMC Biosafety Committee (GMO permit 08-129).

Light microscopical detection of Luc2 and copGFP co-expression

Luc2 expression in transduced HFBSCs was assessed in real time using a purpose-built bioluminescence microscope, at P10 and P15. D-luciferin (potassium salt; Synchem, Felsberg, Germany) was added at a final concentration of 0.1 mM. The bioluminescent signal was recorded for 15 minutes and digital images were acquired using Image-Pro® Plus software, followed by conversion of the grayscale images into pseudocolor images.

Cellular copGFP expression was examined immediately following transduction (P1) and at P5, P10 and P15 using an Olympus IX70 fluorescence microscope (FITC filter settings) equipped with a Leica DFC340 FX digital camera. Digital images were acquired and stored using Leica Application Suite Advanced Fluorescence (LAS AF) software (version 1.9.0). All images were subsequently processed using Adobe® Photoshop® CS6 Extended software (version 13.0 x64).

Proliferation curve

To determine if transduction inhibits cell division and growth, the proliferation rate and doubling time of transduced cells were compared with those of non-transduced control cells during the same passage. Cells were seeded at a density of 1×10^4 cells/well in a PDL-coated 12-well plate and counted after 1 day, 2 and 3 days, using a Luna™ automated cell counter (Logos Biosystems, Anyang City, South Korea). The data were statistically analyzed and plotted in graphs using GraphPad Prism version 6.02 software (GraphPad Software, La Jolla, CA, USA).

Senescence assay

To verify if transduction results in cell immortalization or senescence, the proportion of senescent cells in cultures of transduced HFBSCs was determined using the Senescence Cells Histochemical Staining Kit (Sigma-Aldrich), which is based upon histochemical detection of senescence-associated lysosomal β-galactosidase activity. The assay was performed according to the manufacturer's guidelines.

Cells from P1 (directly after transduction), P3, P9 and P15 were seeded at a density of 1×10^4 cells/well in PDL-coated 12-well plates and allowed to attach. After 24 hours, medium was aspirated and cells were washed twice with PBS and fixed in 2% formaldehyde and 0.2% glutaraldehyde in PBS at room temperature for 7 minutes. Next, the cells were rinsed thrice with PBS and incubated in staining solution at pH 6.0 and 37°C for 24 hours, after which it was replaced with PBS. The staining solution contained 5-bromo-4-chloro-3-indolyl-β-D-galactopyranoside (X-gal; 1 mg/mL). Cells expressing β-galactosidase activity (blue staining) as well as the total number of cells were counted, and the percentage of senescent cells was calculated.

Loading of HFBSCs with NEO-STEM™ TMSR50 nanoparticles

Transduced HFBSCs were loaded with NEO-STEM™ TMSR50 nanoparticles (Biterials, Seoul, South Korea) according to the manufacturer's protocol. Nanoparticles were concentrated by centrifugation ($12,700 \times g$, 10 minutes), dispersed in BGM solution at a concentration of 0.2 mg/mL and, then, sonicated in a bath-type sonicator

(30 kHz, 10 minutes) in order to prevent particle aggregation.

Cells were seeded in PDL-coated 12-well plates at densities of 1×10^4 and 7.5×10^4 cells/well, and incubated with the suspension of TMSR50 nanoparticles for 24 hours, followed by washing with PBS three times and adding fresh pre-warmed (37°C) BGM solution. To investigate the amount of exocytosed nanoparticles over time, medium was collected directly after loading, after 48 hours, 72 hours and 96 hours. Levels of red fluorescence were measured using the SpectraMax Gemini microplate reader (λ_{ex}: 544 nm; λ_{em}: 590 nm; Molecular Devices, Sunnyvale, CA, USA) and analyzed by comparison to a calibration curve.

For prolonged retention, cells were cultured for 7 days, and on alternate days half of the medium was replaced with fresh pre-warmed medium. The cells were examined after 1 day, 3 and 7 days for red fluorescence, due to the rhodamine B isothiocyanate dye from the TMSR50 nanoparticles, with an Olympus IX70 fluorescence microscope (Cy3 filter settings). Images were acquired and digitally stored using LAS AF software. All images were processed using Adobe® Photoshop® CS6 Extended software (version13.0 x64).

Bioluminescent caspase activity assays

To exclude that TMSR50 nanoparticles induce apoptosis in transduced HFBSCs, caspase-3/7 and caspase-9 activities were determined using the Caspase-Glo® 3/7 and Caspase-Glo® 9 bioluminescence-based assay kits, respectively (Promega Corporation, Madison, WI, USA). The assays were performed according to the manufacturer's guidelines with slight modifications.

After centrifugation, transduced HFBSCs were resuspended in BGM containing TMSR50 nanoparticles (0.2 mg/mL) and seeded at a density of 5×10^3 cells/well in a PDL-coated black-walled 96-well microplate (Greiner Bio-One, Kremsmünster, Austria) and allowed to attach for 30 minutes followed by incubation with the respective Caspase-Glo® substrates (caspase-3/7: Z-DEVD-aminoluciferin; caspase-9: Z-LEHD-aminoluciferin) according to the manufacturer's instructions. Bioluminescence was measured directly after seeding and after 4, 8, 16, and 24 hours. Images were acquired for 30 seconds using an IVIS® Spectrum multimodal

imaging system (PerkinElmer, Waltham, MA, USA) with the following settings: open filter, field of view (FOV) C (default setting), f/stop = 1, and medium binning. Image acquisition and analysis were performed with Living Image® version 3.1 software (PerkinElmer). A linear mixed model was fitted to compensate for missing values using SPSS Statistics version 20.0.0.1 software (IBM Corporation, Armonk, NY, USA). GraphPad Prism 6.02 was utilized for additional analysis of the data and plotting of the corresponding graphs.

MTS tetrazolium reduction assay

Cell viability of transduced, nanoparticle-loaded HFBSCs was determined using the colorimetric MTS assay. This assay is based upon the one-step reduction of the colorless tetrazolium compound MTS (3-(4,5-dimethylthiazol-2-yl)-5-(3-carboxymethophenyl)-2-(4-sulfophenyl)-2H-tetrazolium) to a water-soluble colored formazan (blue) in the presence of phenazine ethosulphate. Transduced HFBSCs loaded with TMSR50 nanoparticles and non-loaded control cells were seeded in PDL-coated Corning® Costar® 96-well cell culture plates. After 1 day, 8 and 15 days, cell viability was determined using the CellTiter® 96 AQueous One Solution Cell Proliferation Assay (Promega Corporation) according to the manufacturer's protocol. Colorimetric measurements were performed after a 90-minute incubation period, and 5 seconds shaking, using a VersaMax™ ELISA microplate reader (Molecular Devices, Sunnyvale, CA, USA) at 490 nm. Data acquisition and analysis were performed with SoftMax™ Pro version 5.4.1 software (Molecular Devices).

Differentiation of TMSR50-loaded HFBSCs

Both, transduced HFBSCs loaded with TMSR50 nanoparticles and untreated control cells, were differentiated according to the protocol by Gho *et al*. [38]. Briefly, 2.5 × 10^5 cells were seeded via the side into PDL-coated wells containing PDL-coated cover glasses (Thermo Scientific, Waltham, MA, USA). Differentiation was induced by removal of 250 µL medium and replacement with 300 µL induction medium (IM) consisting of DMEM/Ham's F-12 1:1 supplemented with 1.5 mM cAMP (Sigma-Aldrich), 1% glutamax (Life Technologies), 10 ng/mL NGF, 10 ng/mL GDNF, 10 ng/mL BDNF (all from R&D Systems) and 2% B27 + VitA (Life Technologies).

1

2

3

4

5

6

7

8

A

Subsequently, cultures were allowed to differentiate for at least 60 hours without disturbance followed by removal of 250 μL medium and again substituted with 300 μL IM.

In vitro bioluminescence imaging

The bioluminescent signal of luciferase-expressing cells can be used as a proxy for cell viability, by reason of the fact that the luciferase reaction requires O_2 and ATP. Transduced HFBSCs with and without TMSR50 nanoparticles were seeded in PDL-coated black-walled 96-well microplates (Greiner Bio-One). After 1 day, 8 and 15 days, bioluminescence was recorded after addition of D-luciferin at a final concentration of 0.5 mM. Bioluminescence was measured with an IVIS® Spectrum multimodal imaging system (PerkinElmer) using 30-second acquisition times, open filter, field of view C (default setting), f/stop = 1, and medium binning. Image acquisition and analysis were performed with Living Image® version 3.1 software (PerkinElmer). All images were subsequently processed using Adobe® Photoshop® CS6.

MRI of agarose-embedded TMSR50-loaded HFBSCs

A cell dilution series was done to establish the amount of TMSR50-loaded HFBSCs needed to reach signal threshold for MRI. For this purpose, a multi-layered cell-gradient agarose phantom was fabricated consisting of four layers of agarose-embedded cells at different concentrations, with each cell layer being sandwiched between two acellular agarose layers. Different amounts of cells (5×10^7, 5×10^6, 5×10^5, and 5×10^4 cells/ml) were suspended in a solution of 0.5% agarose (molecular grade; Bioline, London, UK) in PBS. Warm agarose was pipetted, free of air bubbles, into a 50-mL tube. After gelation at -20°C, 20 μL of a cell suspension was mixed with an equal volume of warm agarose and pipetted on top of the solidified agarose bottom layer and left to solidify followed by pipetting 2 mL of agarose on top of the agarose-embedded cell layer. This procedure was repeated several times resulting in four layers containing 1×10^6, 1×10^5, 1×10^4, and 1×10^3 cells/layer. Next, another two layers of 2 mL acellular agarose were created, before filling up the 50-mL tube with agarose. Finally, it was sealed with a layer of Parafilm® M sealing film

before affixing the lid. The phantom was examined for red fluorescence due to the TMSR50 nanoparticles using an IVIS® Spectrum multimodal imaging system at a minimal acquisition time of 1 second (λ_{ex}: 535 nm; λ_{em}: 580 nm). Image acquisition and analysis were performed with Living Image® version 3.1 software.

MRI was performed with a 7-T Bruker PharmaScan® 70/16 (Bruker Biospin, Ettlingen, Germany) equipped with a BGA-9S 300 mT/m gradient system and a conventional 38-mm birdcage transmit-and-receive radio-frequency (RF) coil (Bruker Biospin).

The cell-loaded agarose phantom was placed in the RF coil assembly fixed at the scanner's isocenter and, after an initial localization scan, T2*-weighted three-dimensional fast low-angle shot (FLASH) sequences were used to visualize the different cell layers within the phantom. Optimal sequence parameters were as follows: recovery time (TR): 100 ms; effective echo time (TE): 13 ms; imaging matrix size: 128 x 128 x 64; final voxel resolution of: 0.219 x 0.219 x 25 µm; and a FOV of: 28 x 28 x 16 mm. Data acquisition, image reconstruction and visualization were done with Paravision® 5.1 software (Bruker Biospin).

Statistical analyses

Statistical analyses of the data were performed using GraphPad Prism 6.02 and SPSS Statistics version 20.0.0.1 software (IBM Corporation).

Acknowledgments

Declaration of interest

No conflict of interest has been declared.

Copyright

References

1. Kassem, M., Mesenchymal stem cells: Biological characteristics and potential clinical applications. Cloning Stem Cells, 2004. **6**: pp. 369-374.
2. Schilling, T., Noth, U., Klein-Hitpass, L., Jakob, F., and Schutze, N., Plasticity in adipogenesis and osteogenesis of human mesenchymal stem cells. Mol. Cell Endocrinol., 2007. **271**: pp. 1-17.
3. Andrews, E.M., Tsai, S.Y., Johnson, S.C., Farrer, J.R., Wagner, J.P., Kopen, G.C., and Kartje, G.L., Human adult bone marrow-derived somatic cell therapy results in functional recovery and axonal plasticity following stroke in the rat. Exp. Neurol., 2008. **211**: pp. 588-592.
4. Kim, S.S., Yoo, S.W., Park, T.S., Ahn, S.C., Jeong, H.S., Kim, J.W., Chang, D.Y., Cho, K.G., Kim, S.U., Huh, Y., Lee, J.E., Lee, S.Y., Lee, Y.D., and Suh-Kim, H., Neural induction with neurogenin1 increases the therapeutic effects of mesenchymal stem cells in the ischemic brain. Stem Cells, 2008. **26**: pp. 2217-2228.
5. Muller, J., Ossig, C., Greiner, J.F., Hauser, S., Fauser, M., Widera, D., Kaltschmidt, C., Storch, A., and Kaltschmidt, B., Intrastriatal transplantation of adult human neural crest-derived stem cells improves functional outcome in Parkinsonian rats. Stem Cells Transl. Med., 2015. **4**: pp. 31-43.
6. Sato, T. and Clevers, H., Growing organoids from stem cells. Cell, 2015. **161**: pp. 1700-1701.
7. Lee, S., Choi, E., Cha, M.-J., and Hwang, K.-C., Cell adhesion and long-term survival of transplanted mesenchymal stem cells: A prerequisite for cell therapy. Oxid. Med. Cell. Longev., 2015. **2015**: pp. 632902.
8. Green, A.A. and McElroy, W.D., Crystalline firefly luciferase. Biochim. Biophys. Acta, 1956. **20**: pp. 170-176.
9. Contag, C.H. and Bachmann, M.H., Advances in *in vivo* bioluminescence imaging of gene expression. Annu. Rev. Biomed. Eng., 2002. **4**: pp. 235-260.
10. Mezzanotte, L., Que, I., Kaijzel, E., Branchini, B., Roda, A., and Löwik, C., Sensitive dual color *in vivo* bioluminescence imaging using a new red codon optimized firefly luciferase and a green click beetle luciferase. PLoS ONE, 2011. **6**: pp. e19277.
11. Wilson, B.C., Jeeves, W.P., and Lowe, D.M., *In vivo* and *post mortem* measurements of the attenuation spectra of light in mammalian tissues. Photochem. Photobiol., 1985. **42**: pp. 153-162.
12. Mezzanotte, L., Fazzina, R., Michelini, E., Tonelli, R., Pession, A., Branchini, B., and Roda, A., *In vivo* bioluminescence imaging of murine xenograft cancer models with a red-shifted thermostable luciferase. Mol. Imaging Biol., 2010. **12**: pp. 406-414.
13. Welsh, D.K. and Noguchi, T., Cellular bioluminescence imaging. Cold Spring Harb. Protoc., 2012. **2012**: pp. 852-866.
14. Shimomura, O., Johnson, F.H., and Saiga, Y., Extraction, purification and properties of aequorin, a bioluminescent protein from the luminous hydromedusan, *Aequorea*. J. Cell. Comp. Physiol., 1962. **59**: pp. 223-239.
15. Tsien, R.Y., The green fluorescent protein. Annu. Rev. Biochem., 1998. **67**: pp. 509-544.
16. Shaner, N.C., Steinbach, P.A., and Tsien, R.Y., A guide to choosing fluorescent proteins. Nat. Methods, 2005. **2**: pp. 905-909.
17. Chudakov, D.M., Matz, M.V., Lukyanov, S., and Lukyanov, K.A., Fluorescent proteins and their applications in imaging living cells and tissues. Physiol. Rev., 2010. **90**: pp. 1103-1163.
18. Shagin, D.A., Barsova, E.V., Yanushevich, Y.G., Fradkov, A.F., Lukyanov, K.A., Labas, Y.A., Semenova, T.N., Ugalde, J.A., Meyers, A., Nunez, J.M., Widder, E.A., Lukyanov, S.A., and Matz, M.V., GFP-like proteins as ubiquitous metazoan superfamily: Evolution of functional features and structural complexity. Mol. Biol. Evol., 2004. **21**: pp. 841-850.
19. Hunt, M.E., Scherrer, M.P., Ferrari, F.D., and Matz, M.V., Very bright green fluorescent proteins from the pontellid copepod *Pontella mimocerami*. PLoS ONE, 2010. **5**: pp. e11517.
20. Evdokimov, A.G., Pokross, M.E., Egorov, N.S., Zaraisky, A.G., Yampolsky, I.V., Merzlyak, E.M., Shkoporov, A.N., Sander, I., Lukyanov, K.A., and Chudakov, D.M., Structural basis for the fast maturation of *Arthropoda* green fluorescent protein. EMBO Rep., 2006. **7**: pp. 1006-1012.
21. Jendelova, P., Herynek, V., DeCroos, J., Glogarova, K., Andersson, B., Hajek, M., and Sykova, E., Imaging the fate of implanted bone marrow stromal cells labeled with superparamagnetic nanoparticles. Magn. Reson. Med., 2003. **50**: pp. 767-776.
22. Bulte, J.W. and Kraitchman, D.L., Iron oxide MR contrast agents for molecular and cellular imaging. NMR Biomed., 2004. **17**: pp. 484-499.
23. Sykova, E. and Jendelova, P., In vivo *tracking of stem cells in brain and spinal cord injury*, in *Progr. Brain Res.*, T.W. John and I.R.M. Andrew, Editors. 2007, Elsevier. pp. 367-383.
24. Kallur, T., Farr, T.D., Bohm-Sturm, P., Kokaia, Z., and Hoehn, M., Spatio-temporal dynamics, differentiation and viability of human neural stem cells after implantation into neonatal rat brain. Eur. J. Neurosci., 2011. **34**: pp. 382-393.
25. Kim, J.S., Yoon, T.J., Yu, K.N., Noh, M.S., Woo, M., Kim, B.G., Lee, K.H., Sohn, B.H., Park, S.B., Lee, J.K., and Cho, M.H., Cellular uptake of magnetic nanoparticle is mediated through energy-dependent endocytosis in A549 cells. J. Vet. Sci., 2006. **7**: pp. 321-326.
26. Yoon, T.J., Yu, K.N., Kim, E., Kim, J.S., Kim, B.G., Yun, S.H., Sohn, B.H., Cho, M.H., Lee, J.K., and Park, S.B., Specific targeting, cell sorting, and bioimaging with smart magnetic silica core-shell nanomaterials. Small, 2006. **2**: pp. 209-215.
27. Hwang do, W., Ko, H.Y., Kim, S.K., Kim, D., Lee, D.S., and Kim, S., Development of a quadruple imaging modality by using nanoparticles. Chemistry, 2009. **15**: pp. 9387-9393.
28. Park, K.S., Tae, J., Choi, B., Kim, Y.S., Moon, C., Kim, S.H., Lee, H.S., Kim, J., Kim, J., Park, J., Lee, J.H., Lee, J.E., Joh, J.W., and Kim, S., Characterization, *in vitro* cytotoxicity assessment, and *in vivo* visualization of multimodal, RITC-labeled, silica-coated magnetic nanoparticles for labeling human cord blood-derived mesenchymal stem cells. Int. J. Nanomedicine, 2010. **6**: pp. 263-276.
29. Sieber-Blum, M., Grim, M., Hu, Y.F., and Szeder, V., Pluripotent neural crest stem cells in the adult hair follicle. Dev. Dyn., 2004. **231**: pp. 258-269.

30. Yu, H., Fang, D., Kumar, S.M., Li, L., Nguyen, T.K., Acs, G., Herlyn, M., and Xu, X., Isolation of a novel population of multipotent adult stem cells from human hair follicles. Am. J. Pathol., 2006. **168**: pp. 1879-1888.
31. Krejci, E. and Grim, M., Isolation and characterization of neural crest stem cells from adult human hair follicles. Folia. Biol. (Praha), 2010. **56**: pp. 149-157.
32. Yu, H., Kumar, S.M., Kossenkov, A.V., Showe, L., and Xu, X., Stem cells with neural crest characteristics derived from the bulge region of cultured human hair follicles. J Invest Dermatol 2010. **130**: pp. 1227-36.
33. Liu, F., Zhang, C., and Hoffman, R.M., Nestin-expressing stem cells from the hair follicle can differentiate into motor neurons and reduce muscle atrophy after transplantation to injured nerves. Tissue Eng. Part A, 2014. **20**: pp. 656-662.
34. Mezzanotte, L., Aswendt, M., Tennstaedt, A., Hoeben, R., Hoehn, M., and Löwik, C., Evaluating reporter genes of different luciferases for optimized *in vivo* bioluminescence imaging of transplanted neural stem cells in the brain. Contrast Media Mol. Imaging, 2013. **8**: pp. 505-513.
35. Liu, H.S., Jan, M.S., Chou, C.K., Chen, P.H., and Ke, N.J., Is green fluorescent protein toxic to the living cells? Biochem. Biophys. Res. Commun., 1999. **260**: pp. 712-717.
36. Goto, H., Yang, B., Petersen, D., Pepper, K.A., Alfaro, P.A., Kohn, D.B., and Reynolds, C.P., Transduction of green fluorescent protein increased oxidative stress and enhanced sensitivity to cytotoxic drugs in neuroblastoma cell lines. Mol. Cancer Ther., 2003. **2**: pp. 911-917.
37. McGinley, L., McMahon, J., Strappe, P., Barry, F., Murphy, M., O'Toole, D., and O'Brien, T., Lentiviral vector mediated modification of mesenchymal stem cells & enhanced survival in an *in vitro* model of ischaemia. Stem Cell Res. Ther., 2011. **2**: pp. 12.
38. Gho, C.G., Schomann, T., De Groot, S.C., Frijns, J.H.M., Rivolta, M.N., Neumann, M.H., and Huisman, M.A., Isolation, expansion and neural differentiation of stem cells from human plucked hair: A further step towards autologous nerve recovery. Cytotechnology, 2016. **68**: pp. 1849-1858.
39. Kai, W., Xiaojun, X., Ximing, P., Zhenqing, H., and Qiqing, Z., Cytotoxic effects and the mechanism of three types of magnetic nanoparticles on human hepatoma BEL-7402 cells. Nanoscale Res. Lett., 2011. **6**: pp. 480.
40. Kircher, M.F., Allport, J.R., Graves, E.E., Love, V., Josephson, L., Lichtman, A.H., and Weissleder, R., *In vivo* high resolution three-dimensional imaging of antigen-specific cytotoxic T-lymphocyte trafficking to tumors. Cancer Res., 2003. **63**: pp. 6838-6846.
41. Foster-Gareau, P., Heyn, C., Alejski, A., and Rutt, B.K., Imaging single mammalian cells with a 1.5 T clinical MRI scanner. Magn. Reson. Med., 2003. **49**: pp. 968-971.
42. Yeum, C.E., Park, E.Y., Lee, S.B., Chun, H.J., and Chae, G.T., Quantification of MSCs involved in wound healing: Use of SIS to transfer MSCs to wound site and quantification of MSCs involved in skin wound healing. J. Tissue Eng. Regen. Med., 2013. **7**: pp. 279-291.
43. Okazaki, Y., Rao, S., Asao, S., Tateishi, T., Katsuda, S.-i., and Furuki, Y., Effects of Ti, Al and V concentrations on cell viability. Mater. Trans., 1998. **39**: pp. 1053-1062.
44. Brunner, T.J., Wick, P., Manser, P., Spohn, P., Grass, R.N., Limbach, L.K., Bruinink, A., and Stark, W.J., *In vitro* cytotoxicity of oxide nanoparticles: Comparison to asbestos, silica, and the effect of particle solubility. Environ. Sci. Technol., 2006. **40**: pp. 4374-4381.
45. El Seady, R., Huisman, M.A., Löwik, C.W., and Frijns, J.H.M., Uncomplicated differentiation of stem cells into bipolar neurons and myelinating glia. Biochem. Biophys. Res. Commun., 2008. **376**: pp. 358-362.

Lentiviral transduction and subsequent loading with nanoparticles do not affect cell viability and proliferation in hair-follicle-bulge-derived stem cells *in vitro*

1

2

3

4

5

6

7

8

A